Available online at www.sciencedirect.com
SCIENCE DIRECT
Chemical Physics Letters 418 (2006) 540–543
CHEMICAL PHYSICS LETTERS
www.elsevier.com/locate/cplett

Three-dimensional real-space crystallography of MCM-48 mesoporous silica revealed by scanning transmission electron tomography

Timothy J.V. Yates [a], John Meurig Thomas [a,b,*], Jose-Jesus Fernandez [c,d,1], Osamu Terasaki [e,2], Ryong Ryoo [f,3], Paul A. Midgley [a,*]

[a] Department of Materials Science and Metallurgy, University of Cambridge, Pembroke Street, Cambridge CB2 3QZ, UK
[b] Davy-Faraday Research Laboratory, Royal Institution of Great Britain, 21 Albemarle Street, London W1X 4BS, UK
[c] Department of Computer Architecture and Electronics, University of Almeria, 04120 Almeria, Spain
[d] MRC Laboratory of Molecular Biology, Hills Road, Cambridge CB2 2QH, UK
[e] Department of Structural Chemistry, Arrenhius Laboratory, Stockholm University, 10691 Stockholm, Sweden
[f] National Creative Research Centre for Functional Nanomaterials, Korea Advanced Institute of Science and Technology, Daejeon 305-701, Korea

Received 23 September 2005
Available online 1 December 2005

Abstract

High-angle annular dark-field scanning transmission electron tomography has been used to reveal the three-dimensional lattice structure of the mesoporous silica MCM-48. The incoherent nature of the dark-field signal leads to directly interpretable images and three-dimensional tomographic reconstructions. The ability to manipulate the three-dimensional reconstruction allows the structure to be visualised at any orientation, revealing detail in projection or as slices not hitherto seen by direct imaging techniques.

1. Introduction

The advent of ordered mesoporous silicas [1] has transformed the scope of heterogeneous catalysts principally because the pores, which may be unidirectional or intersecting, are sufficiently large (1.5–30 nm diameter) to allow the passage of reactant and product molecules that cannot be accommodated by any natural or synthetic zeolitic catalyst [2]. These are solids with extremely high surface areas that allow relatively large precursor, mixed-metal carbonylates (e.g., $Pd_6Ru_6(CO)_{24}^{2-}$) to be distributed over the surface, thereby making it possible to prepare nanoparticle bimetallic catalysts (e.g., Pd_6Ru_6) of high activity and selectivity in the hydrogenation of a range of key organic molecules [3]. Despite their enormous potential, the structure of these silica systems is still open to question. Conventional electron microscopy may not always yield the full structure of such systems and so here we turn to electron tomography to reveal the full three-dimensional crystallography of one of these ordered silicas, MCM-48.

Unlike conventional electron microscopy which provides only a two-dimensional projection of a three-dimensional object, electron tomography is able to reveal the full three-dimensional structure by acquiring a series of images from different directions (normally about a single tilt axis) to then merge into a three-dimensional reconstruction, or 'tomogram'. We have shown previously that by using scanning transmission electron microscopy (STEM) and recording high-angle annular dark-field (HAADF) images with electrons scattered to high angles (Rutherford-type scattering) using an annular detector [4], tomographic reconstruction artefacts from Fresnel diffraction and diffraction contrast are minimised because of the loss of transverse coherence in electrons scattered to high angles

* Corresponding authors. Fax: +44 1223 334567.
E-mail addresses: tjvy2@cam.ac.uk (T.J.V. Yates), jmt2@cam.ac.uk (J.M. Thomas), jjfdez@ual.es (J.-J. Fernandez), terasaki@struc.su.se (O. Terasaki), rryoo@kaist.ac.kr (R. Ryoo), pam33@cam.ac.uk (P.A. Midgley).
[1] Fax: +34 950 01 54 86.
[2] Fax: +34 468 16 31 18.
[3] Fax: +82 428698130.

0009-2614/$ - see front matter © 2005 Elsevier B.V. All rights reserved.
doi:10.1016/j.cplett.2005.11.031

[5]. This is particularly important for complex porous systems in which ordered three-dimensional arrangements of pores may be misinterpreted with conventional phase-contrast electron microscopy. To achieve high contrast, a large defocus is often required and, especially at major zone axes, this may lead to some misinterpretation unless careful simulations are computed for comparison. By contrast, STEM HAADF imaging is performed in focus and the interpretation of images acquired this way is considerably more straightforward. As long as the conditions are set correctly, and in particular that the inner angle of the HAADF detector is sufficiently large, pores will always appear as dark contrast and the solid structure bright. In addition, the scattering cross-section is sensitive to the atomic number, Z (in the high-angle limit this is Z^2), making it an ideal imaging mode for many heterogeneous systems.

The three-dimensional ordered cubic variant (with $a = 23$ nm) of the MCM series of mesoporous silicas, known as MCM-48, has a complex gyroid-like three-dimensional pore network; this has been studied previously by two of the authors (OT and RR) using conventional electron crystallography [6]. Structure factors derived from high-resolution phase-contrast electron microscopy were used to determine the MCM-48 silica structure. Here, we reprise that work and consider again the internal structure of MCM-48 based now on a *direct* visualisation of the structure using the incoherent, high-angle scattered electron signal in scanning transmission electron tomography. In addition, because this is a direct 3D *imaging* technique, we are able to reveal any deviation from crystal perfection, including twin boundaries and other extended faults.

2. Experimental

The MCM-48 silica was synthesised using triblock ethylene (EO)–propylene oxide (PO)–EO copolymer Pluronic P123 ($EO_{20}PO_{70}EO_{20}$, $M_{av} = 5800$), butanol and tetraethyl orthosilicate (TEOS) [7]. Care was taken to ensure that all precursor molecules were removed before imaging by a gentle heating of the sample prior to introduction into the electron microscope.

A series of 158 STEM HAADF images was acquired every 1° between −78° and +79° using a 40 mrad detector inner angle. Each image acquired at a magnification of 450 000× was composed of 1024 × 1024 pixels with a pixel size of 0.28 nm and a dwell time of 38 μs per pixel. The series was aligned first by simple cross-correlation and then refined using defects in the supporting carbon film as features with which the alignment procedures could track. Computer memory constraints meant that the data set was re-binned to 512 × 512 and a sub-area of each image was selected for reconstruction using an iterative reconstruction technique (SIRT) implemented in Inspect3D [8]. The resulting tomogram was then processed using a noise-reduction algorithm called anisotropic non-linear diffusion (AND), developed by one of us (JJF), and further adapted to use with tomograms acquired using STEM HAADF imaging [9]. The algorithm is essentially a quasi-intelligent smoothing algorithm in which areas of similar planarity (intensity) or curvature are connected. In other words the tomogram (or image) flux is 'diffused' to maximise the contrast of real features.

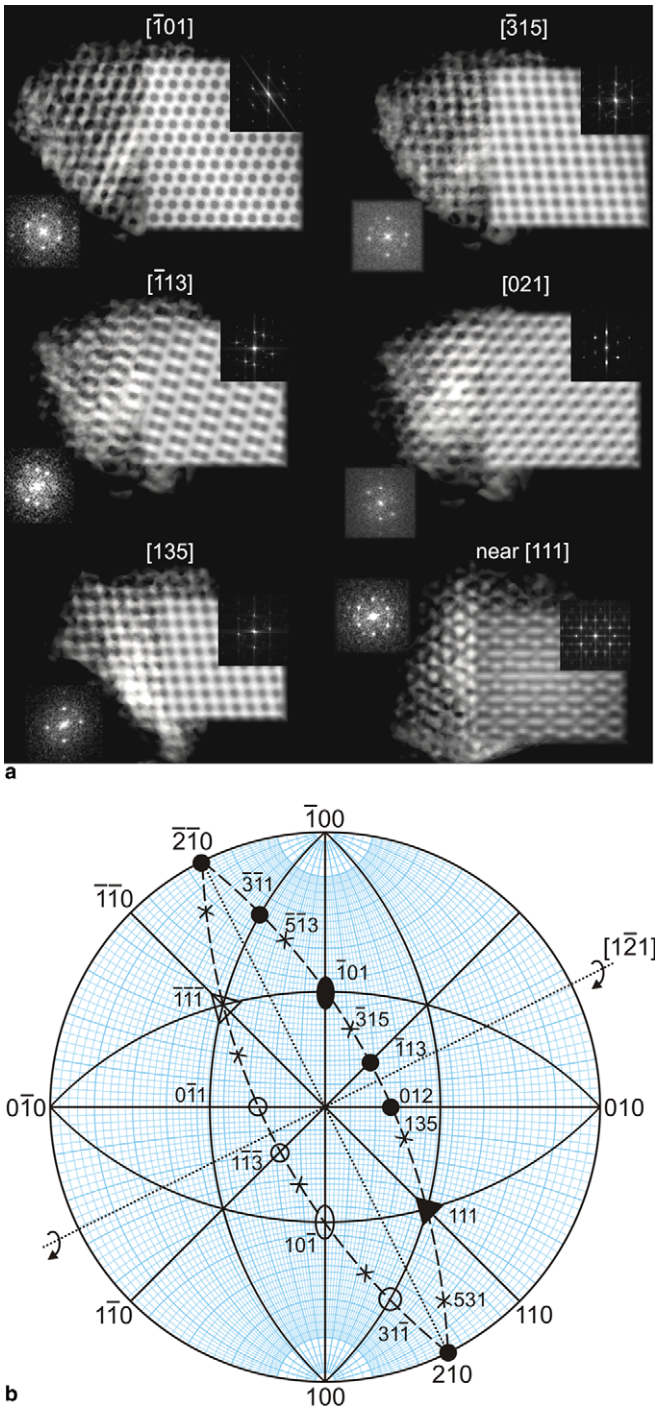

Fig. 1. (a) A montage of tomographic voxel projections of MCM-48 shown at successive major zone axes as the three-dimensional tomographic reconstruction is rotated about a ⟨1 1 2⟩ zone axis. (b) Stereographic representation of the image series shown in (a). Crosses indicate the ⟨1 3 5⟩ axes.

3. Results and discussion

Fig. 1a shows a montage of voxel projections computed from a three-dimensional tomographic reconstruction of a sub-100 nm particle of MCM-48 silica. Each projection is at a major zone axis encountered when rotating about a ⟨1 1 2⟩ axis through a symmetry-independent sector of reciprocal space. A {1 1 2} plane, whose normal is vertical in the plane of the paper, is common to all projections. On the right of each image is a simulation of the MCM-48 structure based on an approximate gyroid surface given by the equation:

$$h(x,y,z) = \sin x \cos y + \sin z \cos x + \sin y \cos z = 0.$$

Power spectra for both experiment and simulation are shown as insets. The agreement between experiment and simulation is remarkably consistent for each projection except near the ⟨1 1 1⟩ axis, which we will discuss later. The ⟨1 3 5⟩ axes contain two dominant sets of {1 1 2} planes, the strongest scattering planes in the lattice. The full 360° rotation about the ⟨1 1 2⟩ axis can be seen in an animation of the reconstruction – see Electronic Supplementary Information.

Although such projections could in principle be acquired through successive images recorded at zone axes found by tilting in the microscope, in practice for MCM-48, which can be prone to beam damage, or for example for interfacial phases or small embedded crystallites, it can be a very difficult and time-consuming task to identify major zone axes in situ. Electron tomography offers a way of recording images about a 'random' tilt axis, performing a three-dimensional reconstruction and then, post facto, aligning the whole crystal in the computer – a far less demanding task than in the electron microscope! In addition, by collecting over a large angular range, access is made possible to almost all major zone axes of interest, which may not be possible, or may be missed, with conventional microscopy.

Fig. 2 shows a reconstructed *slice* perpendicular to a ⟨1 1 0⟩ direction. A Bragg-filtered version, used to reduce non-periodic artefacts, has been superimposed for clarity. A centred projected cell is also shown. The inset shows a power spectrum of the slice indicating strong pairs of Fourier components, which if indexed according to a ⟨1 1 0⟩ diffraction pattern, correspond to {3 3 2} and {2 2 4} reflections, the latter set demonstrating 4.7 nm periodic resolution within the slice. The ability to slice through different planes of the crystal can be of great advantage when visualising complex three-dimensional geometry. An animation of successive ⟨1 1 0⟩ slices can be found in the Electronic Supplementary Information. All projections and slices from the reconstruction (together with the corresponding system-

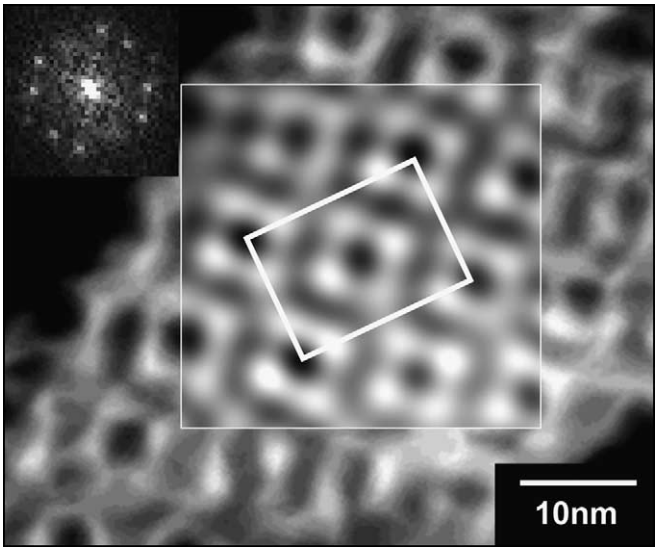

Fig. 2. A reconstructed *slice* through the MCM-48 reconstruction perpendicular to the ⟨1 1 0⟩ zone axis. A Bragg-filtered inset enhanced the periodic detail. The pairs of spots in the power spectrum correspond to {3 3 2} and {2 2 4} reflections. A centred projected cell is outlined in white.

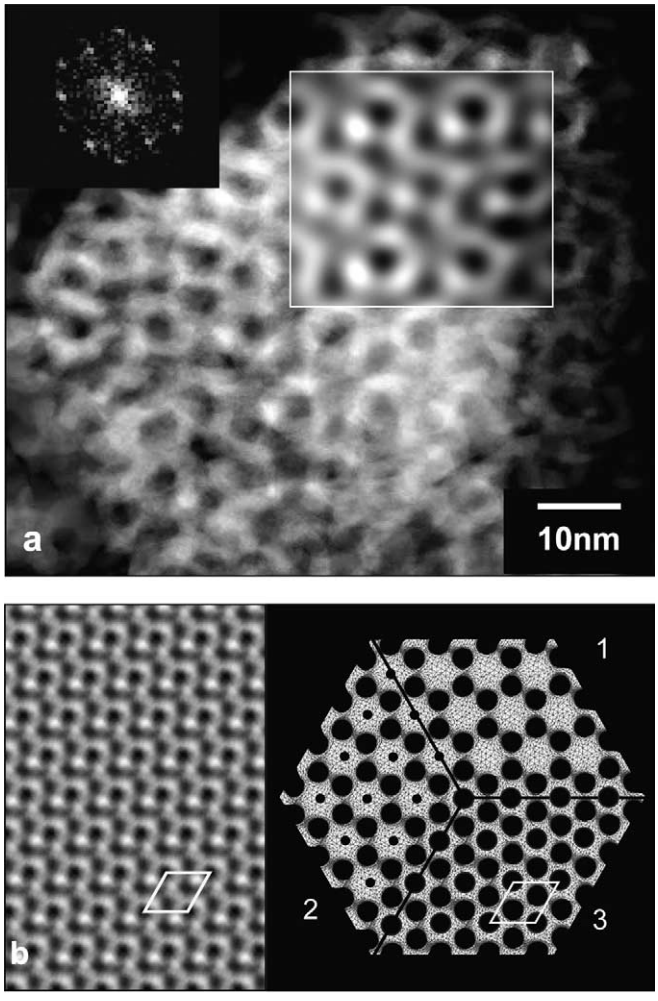

Fig. 3. (a) A ⟨1 1 1⟩ voxel projection of MCM-48. The superposed inset is a Bragg-filtered version revealing a periodic array of large pores. (b) Averaged, tessellated motif from (a) and a schematic diagram indicating (1) the basic gyroid structure, (2) the proposed MCM-48 structure from [6] and (3) a new proposed structure with larger complementary pores. Projected unit cells are outlined in white.

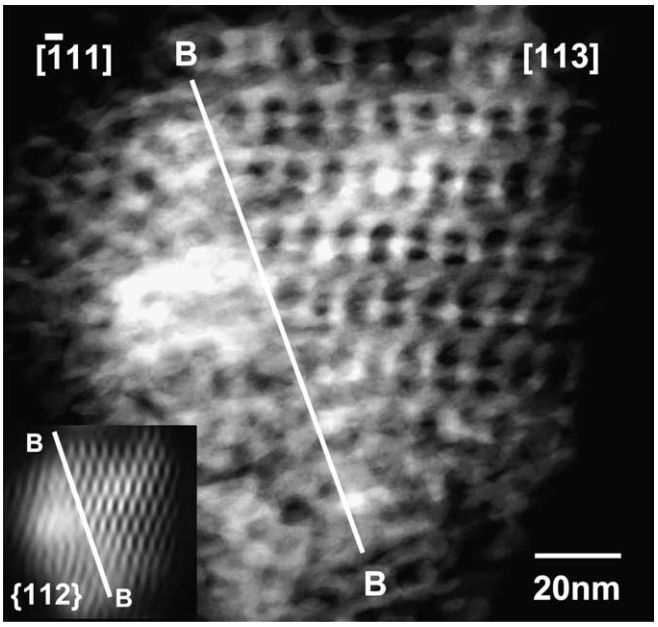

Fig. 4. A view of a boundary (BB) separating two 'grains' of MCM-48 with [1 1 3] orientation (right) and [$\bar{1}$ 1 1] orientation (left). A common set of {1 1 2} planes is seen in the Bragg-filtered inset.

atic absences in the associated power spectra) are consistent with the proposed space group of Ia$\bar{3}$d [6].

The mismatch between experiment and simulation seen near the [1 1 1] zone axis of Fig. 1 is highlighted further in Fig. 3a. Here, we show a projection at a ⟨1 1 1⟩ axis with the pore structure clarified in the Bragg-filtered inset. Fig. 3b shows an average motif derived from (a) and tessellated to form a two-dimensional lattice. No symmetrisation was performed beyond a small correction for geometric image distortion. A comparison between this and the montage of three possible projections down the ⟨1 1 1⟩ axis highlights differences between: (1) the ideal gyroid surface, (2) the array of primary and complementary pores as indicated in [6] and (3) a possible new model for the pore structure of MCM-48 presented here. By studying intensity profiles across the reconstructed projection, it was found that the two sets of pores have the same diameter within experimental error and which we estimate from this work to be 6 nm. In previous studies [6] the complementary pore sizes of MCM-48 were determined based primarily on pore volumes modelled from nitrogen gas adsorption–desorption experiments. In the future, direct structural measurements available with STEM tomography should overcome some of the limitations of such model-dependent analyses.

Fig. 4 shows another strength of a three-dimensional real-space approach to the study of mesoporous structures. Here, we reveal the presence of a boundary apparently separating crystal 'grains' with orientations parallel to the [1 1 3] zone axis on the right-hand side and [$\bar{1}$ 1 1] on the left. One set of {1 1 2} planes is common across the boundary as seen by the inset in the left hand corner of the figure and by the power spectra taken from each side of the boundary. The boundary itself is parallel to a {2 2 0} plane of the left-hand grain and a {1 1 2} plane of the grain on the right. In order for this orientation relationship to be achieved and for the common {1 1 2} plane to be undisturbed across the boundary, there must be a rotation of about 52° between grains, i.e., the angle between the [1 1 3] and [$\bar{1}$ 1 1] zone axes. In principle such a relationship could have been found in situ using conventional microscopy but would have required an element of chance to hit upon the optimum orientation to see the inter-grain relationship. With a three-dimensional tomographic approach, that element of chance is no longer needed.

4. Conclusions

In this Letter, we have shown how with scanning transmission electron tomography it is possible to reveal directly the three-dimensional crystallography of the mesoporous silica, MCM-48. The ability to interrogate the three-dimensional internal structure of ordered materials with near nanometer resolution has important consequences not only for the understanding of many complex catalyst systems but for many structures found in other fields of physical science.

Acknowledgements

The authors acknowledge the financial support of the EPSRC, the Isaac Newton Trust, FEI Company and the Spanish MEC (TIC2002-00228, PR2004-0367).

Appendix A. Supplementary data

Supplementary data associated with this article can be found, in the online version, at doi:10.1016/j.cplett.2005.11.031.

References

[1] C.T. Kresge, M.E. Leonowicz, J. Roth, J.C. Vartuli, J.S. Beck, Nature (London) 359 (1992) 710;
S. Inagaki, Y. Fukishima, K. Kuroda, J. Chem. Soc., Chem. Commun. (1993) 680.
[2] J.M. Thomas, Nature (London) 368 (1994) 289.
[3] W. Zhou, J.M. Thomas, D.S. Shephard, B.F.G. Johnson, T. Maschmeyer, D. Ozkaya, R.G. Bell, Q. Ge, Science 280 (1998) 705.
[4] A. Howie, J. Microsc. 117 (1979) 11.
[5] P.A. Midgley, J.M. Thomas, M. Weyland, B.F.G. Johnson, Chem. Commun. (2001) 907;
P.A. Midgley, M. Weyland, Ultramicroscopy 96 (2003) 413;
J.M. Thomas, P.A. Midgley, T.J.V. Yates, J.S. Barnard, R. Raja, I. Arslan, M. Weyland, Angew. Chem., Int. Ed. 43 (2004) 6745.
[6] Y. Sakamoto, T.-W. Kim, R. Ryoo, O. Terasaki, Angew. Chem., Int. Ed. 43 (2004) 5231.
[7] F. Kleitz, S.H. Choi, R. Ryoo, Chem. Commun. (2003) 2136.
[8] Inspect3D v2.0, FEI Company, Eindoven, The Netherlands. Available from: http://feicompany.com.
[9] J.J. Fernandez, S. Li, J. Struct. Biol. 144 (2003) 152.